Isotopic Raman broadening due to Anderson localization of harmonic phonons in partially deuterated ice VII and VIII

Mungo Frost,[1] Andreas Hermann,[2] Siegfried H. Glenzer,[1] and Graeme J. Ackland[2]
[1]*SLAC National Accelerator Laboratory, 2575 Sand Hill Road, Menlo Park, California 94025, USA*
[2]*Centre for Science at Extreme Conditions and SUPA, School of Physics and Astronomy, University of Edinburgh, Edinburgh EH9 3FD, United Kingdom*

(Received 31 July 2023; accepted 6 November 2023; published 21 November 2023)

Raman spectra from molecular systems are typically regarded as comprising a set of sharp peaks. These arise from both single-molecule modes and extended Γ point phonons being, in theory, harmonic oscillators. Broadening is typically assigned to thermal, linewidth, and anharmonic effects. Here we measure significant broadening in the Raman signal from partially deuterated water ices VII and VIII, which is absent in the pure systems. This isotopic broadening is much greater than any anharmonic effects and is reproduced by lattice dynamics calculations assuming only harmonic bonding. Instead, it arises from mass disorder induced phonon localization. This localization leads to many overlapping modes with a range of frequencies dependant on local isotopic environment and Raman activity due to lack of distinct molecular or crystalline symmetry.

DOI: 10.1103/PhysRevResearch.5.043166

Anderson localization is a phenomenon where lattice disorder disrupts diffusive transport resulting in localization, and has been observed in various systems including visible light [1], electrons [2], and microwaves [3]. It predicts that sufficient disorder in masses, bond strengths [4], or molecular orientation [5–7] causes the wavelike nature of phonons to break down and the vibrations to become localized. Such so-called "phonon localization" was subsequently found in dense hydrogen-deuterium alloys where the large mass difference between the isotopes was sufficient to drive localization [8,9].

Hydrogen and deuterium differ in mass by a factor of almost two, the largest ratio between the stable isotopes of any element. In hydrogen-deuterium mixtures, localization occurs in phases that are only stable at extreme pressures above 200 GPa. These are experimentally challenging to investigate and, consequently, their structures are not certain [8–10]. Here we report the observation of phonon localization in isotopically disordered ice VII and VIII at pressures between 2.5 and 20 GPa. Water ice has been widely studied in this regime [11–15] and its structure is well known which simplifies analyzing the localization. The Raman spectra of natural, 50% deuterated and 99.9% deuterated ices are investigated by combined experiments and density functional theory (DFT), revealing mass disorder induced phonon localization in the isotopically mixed system.

Normal (H_2O) and heavy (D_2O) water have significantly different properties [16,17]. Partially deuterated water undergoes rapid proton/deuteron exchange forming semiheavy water, HOD, via the equilibrium reaction: $H_2O + D_2O <=> 2HOD$. At 25 °C and ambient pressure, the equilibrium constant is 3.86 [18], meaning the concentration of HOD in a 50% deuterated sample is approximately twice that of H_2O or D_2O. Partially deuterated water has been subject to limited investigation, though modifications in the ambient-pressure hydrogen bonding of liquid water [19] and ice Ih [20], and high-pressure viscosity [21] have been studied.

Water has a rich phase diagram with many polymorphs depending on pressure, temperature, and sample history [22], though the phase boundaries vary only sightly with isotopic composition [23]. At room temperature, liquid water freezes to form ice VI at 1 GPa, which then converts to ice VII at 2.1 GPa. Ice VII covers a large area of *PT* space and consists of a body centered cubic array of oxygen atoms tetrahedrally linked by disordered hydrogens such that each oxygen has two donor and two acceptor hydrogen bonds. This forms two interpenetrating, but not interconnected, cubic diamond lattices [15]. Many of the transitions from ice VII to adjacent phases only involve the hydrogen atoms and leave the oxygen lattice intact, for example proton-ordered ice VIII, proton symmetrized ice X, and the plastic and superionic phases at higher temperature [13,15,24–26]. Raman spectroscopy is an ideal probe to study isotope effects on the hydrogen sublattice dynamics.

Here we present high-resolution Raman spectra of normal, 50% deuterated and 99.9% deuterated ice VII from 2.5 to 20 GPa. Accompanying DFT calculations on ice VIII agree closely with the experiment and reveal mass disorder induced vibrational localization to play an important role in the Raman spectra of the partially deuterated system.

Samples were compressed in a diamond anvil cell equipped with low fluorescence diamond anvils with 400 μm culets. Rhenium gaskets were prepared to 120 μm thickness with a 205 μm hole drilled using electrical discharge machining. Pressure was determined via the fluorescence wavelength of

a ruby sphere with an uncertainty of 0.03 GPa [27]. Samples were distilled water, deuterated water (99.9% atom D, Sigma Aldrich), and an equimolar mixture of these. Raman spectra were collected using a 514 nm argon ion laser. Voigt functions were used for peak fitting.

The Raman signal from the diamond anvils must be subtracted where it coincides with features from the sample, for example the O-D stretch in water and second order diamond Raman around 2200 to 2400 cm^{-1}. We used the same anvils for each sample, with gaskets prepared to be as similar as possible, such that the Raman spectrum from normal water, which has no detectable Raman modes coinciding with second order diamond, can be used as a reference at a given pressure. In all cases the measured pressure was within 2% of the target pressure. The success of this method is outlined in Fig. S1 of the Supplemental Material [28].

DFT calculations were performed with the CASTEP code [29], using norm-conserving pseudopotentials generated on the fly and the PBE exchange-correlation functional [30]. Electronic wave functions are expanded in a plane wave basis set (cutoff energy $E_c = 600$ eV, 6x6x6 (4x4x4) k-point grids) for the ice VIII primitive unit cell (16 molecule supercell). Structures of ice VIII were fully optimized at pressures between 0 and 20 GPa.

Raman spectra were simulated for 16-molecule $(\sqrt{2}, \sqrt{2}, 1)$ supercells of ice VIII's conventional unit cell, with harmonic phonon frequencies and Raman intensities obtained from density functional perturbation theory (DFPT) [31]. The 50% and 99.9% deuterated samples were approximated by using cells with 4 H_2O/4 D_2O/8 HOD and 15 D_2O/1 HOD molecules, respectively. For the former, spectra were averaged over 16 random distributions of the molecules in the cell.

In the Raman experiment all samples exhibited the expected phases from liquid to ice VI to ice VII with transition pressures of 1.0 GPa and 2.1 GPa. The Raman spectra of H_2O and D_2O agree with previous results [12,32]. The D_2O sample has a weak Raman peak in the O-H stretch region implying that there is a small quantity of hydrogen present. This peak will be almost entirely due to HOD embedded in D_2O as the vast excess of deuterium will make the concentration of H_2O negligible.

Raman spectra of ice VII were measured between 2.5 and 20 GPa in 2.5 GPa steps and simulated for ice VIII using DFT at 0, 5, 10, 15, and 20 GPa. Ice VIII is a proton-ordered form of ice VII and has a very similar Raman spectrum [33]. Simulating the proton disorder of ice VII in addition to the isotopic disorder, would be computationally challenging for arguably relatively little insight, because our main focus is to show that mass disorder alone causes the localization. Experimentally cooling the sample to measure ice VIII requires the use of a cryostat which reduces the quality of the Raman spectra. It also makes the very tight pressure control required for comparison between isotopic mixture and subtraction of the second order diamond feature from the O-D region extremely challenging. Therefore, ice VIII is used for all calculations while the experiment uses the closely related ice VII. Experimental and simulated Raman spectra at 10 GPa are shown in Fig. 1. Ice VII has three regions of Raman activity detectable in this study, shown in Figs. 1(a) and 1(c). At low shift [Fig. 1(a)] the lattice modes are, within experimental resolution, insensitive to the isotopic makeup of the compounds. As they are dominated by molecular translations and hence by the oxygen mass, this is expected.

At higher shift [Figs. 1(b) and 1(c)]. the O-D and O-H stretches are seen. The isotopically pure samples each exhibit three well defined stretching modes. In contrast, the stretch features of the partially deuterated sample occupy narrower frequency ranges and are asymmetric with a ramp downward upon frequency increase, but otherwise featureless. We interpret this as a result of many overlapping modes with the frequency of each O-H (O-D) stretch depending on the local isotopic composition. Initially, this interpretation is supported by the much narrower symmetric Raman mode arising from HOD embedded in D_2O near 3240 cm^{-1} in the O-H stretch region of the highly deuterated sample. In this case the HOD molecules are too far apart to couple effectively, and instead each O-H bond vibrates in isolation. DFT calculations, discussed below, further support this interpretation, revealing many Raman active phonons in these frequency ranges, with energies and intensities depending on the local isotopic environment.

No Raman modes of ice VII are experimentally observable outside the regions shown in Fig. 1. However, some additional modes are calculated at low to mid frequency but not experimentally observed. This spectral region is shown in Fig. S2 of the Supplemental Material [28]. Similar modes are observed and calculated in the IR spectra of ice VII [34,35], and it is likely that anharmonicity and lifetime broadening effects, which are absent in our DFPT, are responsible for the modes not being observed experimentally. The offset between experimental and simulated peak positions in Fig. 1 is up to 200 cm^{-1} in the O-H stretch region due to anharmonicity effects [36]. However, those effects are mostly due to the intramolecular O-H and O-D covalent bond potential energy surface, so peak spacings and relative intensities (which arise from intermolecular interactions) are much better accounted for at the harmonic DFPT level of theory, and allow for the detailed comparisons between the different isotopic mixtures further below.

The pressure dependence of the Raman shifts are summarized in Fig. 2. The features of the mixed sample are much broader than any individual peak for the pure samples, see Fig. S3 of the Supplemental Material [28] for plotted full width at half maxima (FWHM). This is interpreted as the O-H and O-D stretching Raman features of the isotopically mixed sample consisting of many modes close in energy that are not individually resolvable, so the width of the feature arises from the range of vibrational energies present. This range increases with pressure as increased density leads to stronger interactions between neighboring molecules, and so an increased effect of local isotopic composition on the vibrational frequency of a given O-H bond.

To further understand the vibrational properties, particularly of the isotopic mixture, we performed phonon calculations and simulated Raman/IR intensities on pure H_2O, D_2O, and 50% H:D mixtures. For the latter, we averaged spectra over 16 different isotope distributions in 16-molecule supercells of ice VIII; see Fig. 3(b) for a representative cell. Figures 1(d)–1(f) show simulated spectra at 10 GPa, with all

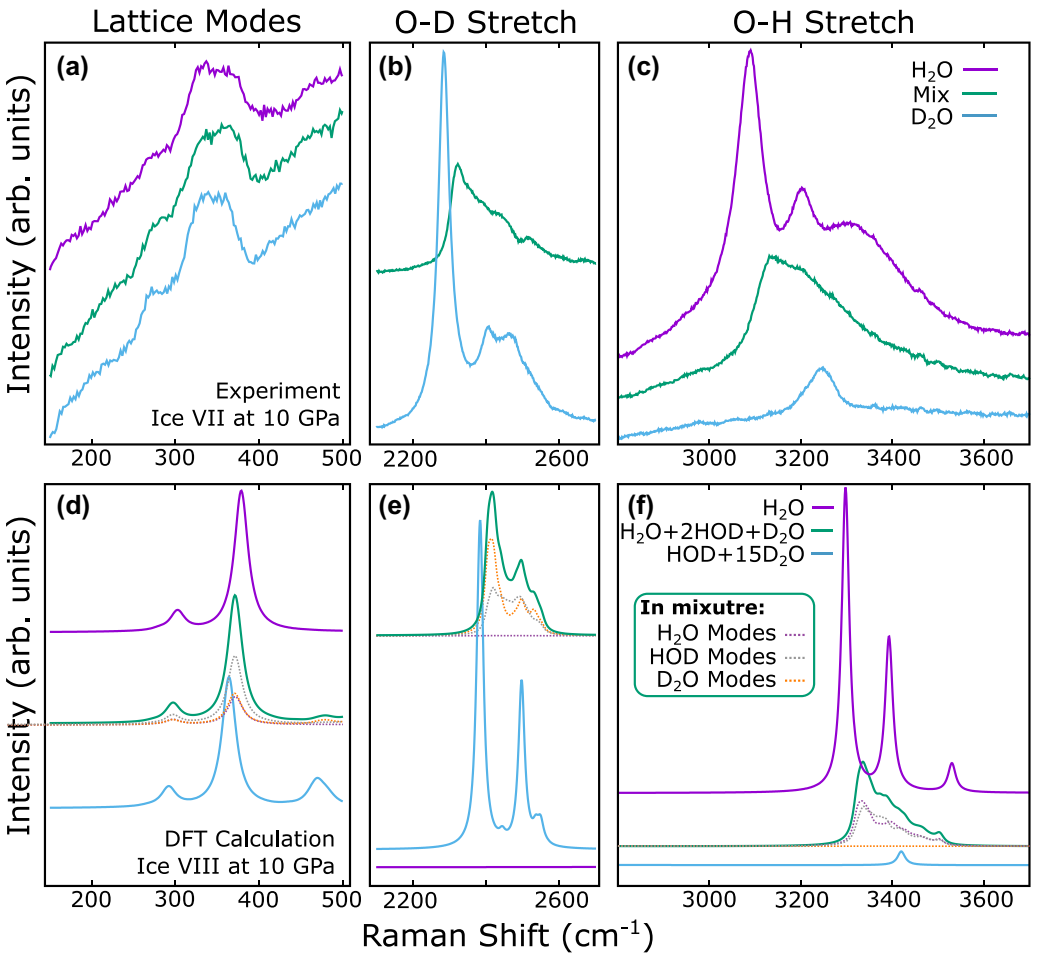

FIG. 1. Raman spectra of ice VII at 10 GPa. (a), (b), (c): the lattice modes, background subtracted O-D stretching region, and O-H stretching region experimentally observed. (d), (e), (f): DFT simulation of the same regions. Intensity scale varies between frames. The dotted lines under the simulated spectra of the isotopically mixed system give the projections of the modes onto each molecular species.

modes displayed as Lorentzians with fixed 10 cm^{-1} linewidth. The spectra agree very well with the experimental data in all three frequency regions. Absolute O-D/O-H stretch frequencies are offset from the experiment, which is an artifact of the exchange-correlation functional [37], but relative peak intensities and isotope effects are captured very well.

We note first that some features of the Raman spectra (such as the characteristic ramp) are not indicative of the overall phonon frequency distribution. In Fig. 3(a) we show the zone-centered phonon density of states (DOS), as well as simulated Raman and IR spectra in Fig. 3(c). In the mixture, the O-D and O-H stretches occupy the same frequency ranges as in pure D_2O and H_2O but are much less peaked, as expected with the loss of clearly defined collective excitations. The Raman spectrum [c.f. Figs. 1(e) and 1(f)] shows the downward ramp with frequency but neither IR nor overall phonon DOS show this. In the bending region (1000–2000 cm^{-1}) a new mode appears in the mixture, due to the presence of HOD species (see also next paragraph). The lattice modes (below 1000 cm^{-1}) are much broader and less defined in the mixture compared to pure H_2O and D_2O. Next, we used the inverse participation ratio [38] to quantify the degree of (de)localization of all phonon modes, $L_\nu = \sum_i (e_{\nu ix}^2 + e_{\nu iy}^2 + e_{\nu iz}^2)^2$, where $e_{\nu i\alpha}$ are the Cartesian components of the normalized displacement vector of mode ν and atom i. L_ν tends to $1/N$ for a mode equally distributed across all atoms, and to one for a mode fully localized on a single atom. Figure 3(d) shows the distributions of L_ν for all three compounds. The modes in pure H_2O and D_2O are, as expected, very delocalized, close to the lower bound of $L_\nu \approx 0.02$. By contrast, for the mixture L_ν has a much broader distribution and a very long tail to large values, i.e., modes are much more localized.

For the isotopically mixed data, we further projected all phonon eigenvectors onto the molecular species—H_2O, D_2O, and HOD. Figures 4(a) and 4(c) shows the resulting projected phonon-DOS and projected Raman intensities. We note that HOD molecules contribute as much as D_2O/H_2O to the O-D/O-H vibron, both for Raman and for the phonon DOS. The three peaks in the bending region (1000–2000 cm^{-1}) are each associated with a specific molecule, and the lattice modes are combinations of all three molecules. Figure 4(b) shows the distribution of L_ν against frequency in the O-D/O-H stretch region (accumulated from all 16 different supercells), and colored by normalized Raman intensity for each mode ν. There is little correlation between mode localization and frequency or Raman intensity. The large number of modes more localized

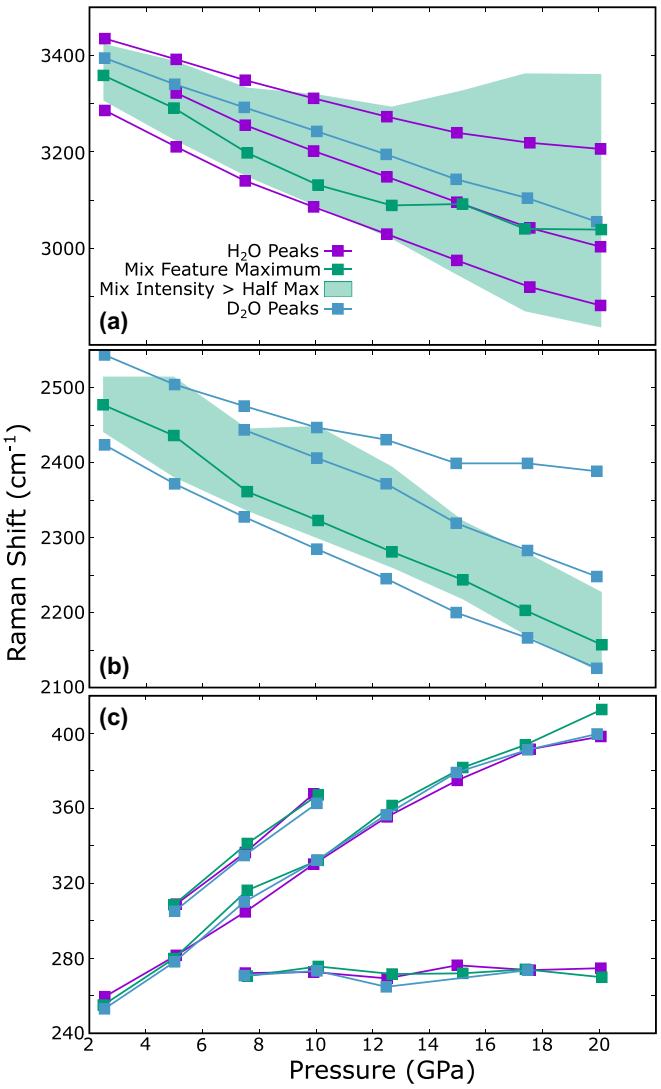

FIG. 2. Experimental ice VII Raman mode frequencies vs. pressure for various isotopic compositions: (a) the O-H stretching region, (b) the O-D stretching region, (c) the lattice modes. Both the maximum intensity and FWHM of the stretching features for 50% deuterated ice are shown, revealing substantial broadening in the O-H stretch region with increased pressure.

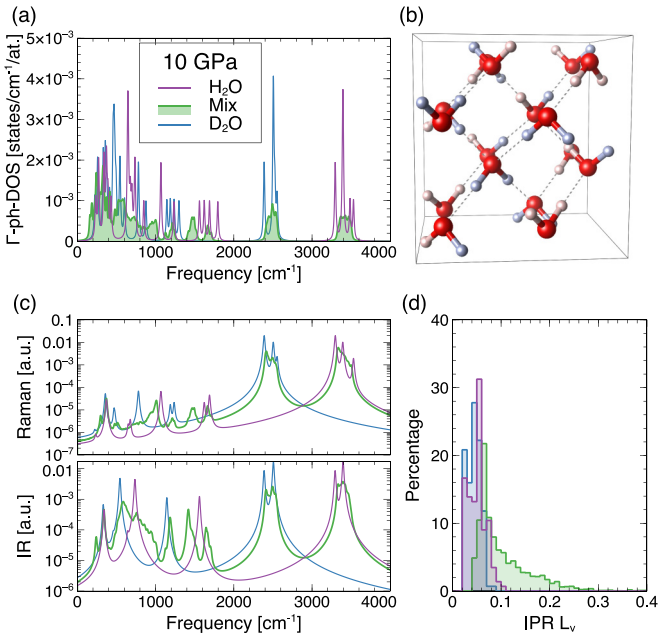

FIG. 3. (a) DFT zone-center phonon DOS's for the ice VIII structure at 10 GPa for H_2O, D_2O, and the 50:50 mixture (averaged over 16 isotope distributions). (b) Example 16-molecule supercell for mixture phonon calculations; O/H/D atoms are red/white/blue spheres. (c) Simulated Raman and IR intensities for the same structures. (d) Inverse participation ratio (IPR) distribution for the phonons of the three compounds.

than in pure H_2O/D_2O ($L_v > 0.1$) spans the entire frequency range of the O-D/O-H stretch regions, leading to the lack of clear features in the spectra. The characteristic ramp shape of the stretches in the mixture is due to a relatively small number of highly Raman active modes at the lower frequency end of each stretch rather than, for instance, a renormalization of phonon modes in the mixture. Those Raman active modes span a range of localization ($0.05 \leqslant L_v \leqslant 0.25$) and involve both the pure D_2O/H_2O species as well as HOD molecules, see Fig. 4(c). As the latter make up 50% of the molecules in the cells, they act to couple the O-D/O-H stretches throughout the lattice.

Finally, we show in Fig. 4(d) the distribution of L_v for the three molecule types, by classifying each phonon mode by the dominant molecule type in its displacement vector e_v. Phonon modes dominated by HOD molecules are significantly less localized than modes dominated by H_2O/D_2O. This suggests that collective excitations are most easily formed by coupling to the HOD sublattice, while modes on H_2O/D_2O cannot so easily span the lattice. Ice VII/VIII comprises two interpenetrating hydrogen-bonded sublattices, each with diamondlike H-bond topology. The percolation threshold for a diamond lattice is 0.43 [39], so the expected HOD occupancy of ~0.5 suggests that excitations delocalized over the HOD network are viable, while those over H_2O and D_2O are not.

In conclusion, we report phonon localization in partially deuterated ice VII/VIII, as isotope effects disrupt the order of hydrogen masses in the crystal lattice. This is the second system in which isotopic Anderson localization of phonons has been observed, the previous being dense hydrogen-deuterium mixtures at pressures in excess of 200 GPa. In contrast to dense hydrogen, ice VII and VIII occur at accessible conditions and have well known crystal structures. DFT calculations are able to reproduce the measured spectra and reveal that many of the O-H (O-D) stretching modes are localized over small clusters of molecules. The observed Raman features arise from many localized modes closely spaced in energy, explaining their appearance. Lower frequency, in-phase vibrations tend to have higher Raman activity, leading to the characteristic ramp shape of the Raman signal. Additionally, HOD molecules couple vibrations between O-H and O-D stretches, and those modes that are dominated by the more abundant HOD molecules are generally less localized, suggesting percolationlike behavior.

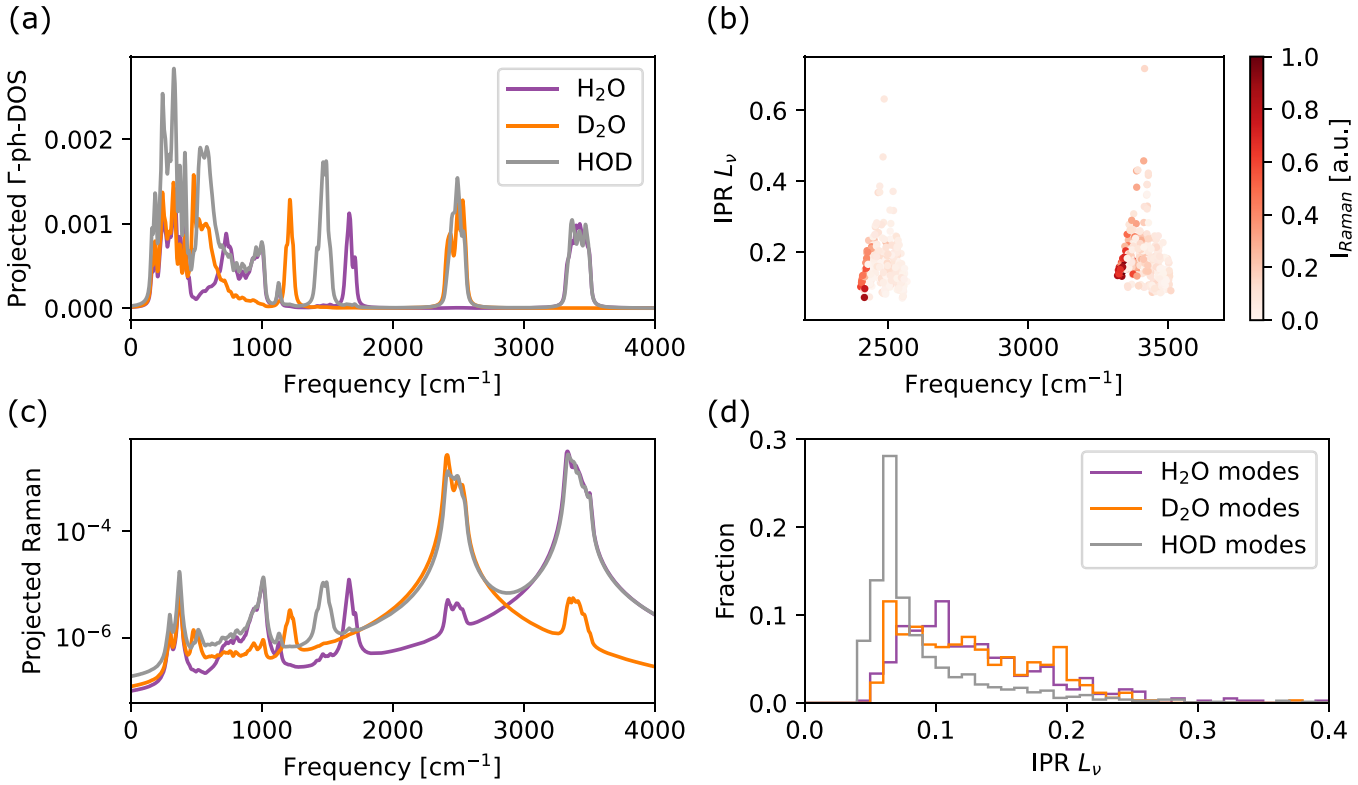

FIG. 4. Analysis of DFT phonon data of the ice VIII 50:50 isotope mixture at 10 GPa, colors refer to molecule type within the partially deuterated ice. (a), (c) Zone-centered phonon DOS and simulated Raman projected onto $H_2O/D_2O/HOD$ molecules. (b) Inverse participation ratio (IPR) L_ν of O-D and O-H vibrons against frequency, shaded by Raman activity (using all data from 16 configurations). (d) Distribution of L_ν, with modes assigned to dominant molecule type.

This work was supported by the DOE Office of Fusion Energy Science Funding No. FWP100866 and No. FWP100182. Computational resources provided by the United Kingdom's National Supercomputer Service through the UKCP consortium (EP/P022561/1) and by the United Kingdom Materials and Molecular Modelling Hub (EP/P020194) are gratefully acknowledged. G.J.A. would like to acknowledge the support of the European Research Council (ERC) Grant "Hecate" Reference No. 695527.

The authors have no conflicts to disclose.

[1] M. Störzer, P. Gross, C. M. Aegerter, and G. Maret, Observation of the critical regime near Anderson localization of light, Phys. Rev. Lett. **96**, 063904 (2006).

[2] A. Pruisken, Universal singularities in the integral quantum hall effect, Phys. Rev. Lett. **61**, 1297 (1988).

[3] A. A. Chabanov, M. Stoytchev, and A. Z. Genack, Statistical signatures of photon localization, Nature (London) **404**, 850 (2000).

[4] C. Monthus and T. Garel, Anderson localization of phonons in dimension d= 1, 2, 3: finite-size properties of the inverse participation ratios of eigenstates, Phys. Rev. B **81**, 224208 (2010).

[5] P. I. C. Cooke, I. B. Magdău, M. Peña-Alvarez, V. Afonina, P. Dalladay-Simpson, X.-D. Liu, R. T. Howie, E. Gregoryanz, and G. J. Ackland, Raman signal from a hindered hydrogen rotor, Phys. Rev. B **102**, 064102 (2020).

[6] P. I. C. Cooke, I. B. Magdău, and G. J. Ackland, Calculating the raman signal beyond perturbation theory for a diatomic molecular crystal, Comput. Mater. Sci. **210**, 111400 (2022).

[7] M. Peña-Alvarez, V. Afonina, P. Dalladay-Simpson, X.-D. Liu, R. T. Howie, P. I. C. Cooke, I. B. Magdau, G. J. Ackland, and E. Gregoryanz, Quantitative rotational to librational transition in dense H_2 and D_2, J. Phys. Chem. Lett. **11**, 6626 (2020).

[8] R. T. Howie, I. B. Magdău, A. F. Goncharov, G. J. Ackland, and E. Gregoryanz, Phonon localization by mass disorder in dense hydrogen-deuterium binary alloy, Phys. Rev. Lett. **113**, 175501 (2014).

[9] I. B. Magdău and G. J. Ackland, Infrared peak splitting from phonon localization in solid hydrogen, Phys. Rev. Lett. **118**, 145701 (2017).

[10] C. J. Pickard, M. Martinez-Canales, and R. J. Needs, Density functional theory study of phase IV of solid hydrogen, Phys. Rev. B **85**, 214114 (2012).

[11] M. Somayazulu, J. Shu, C.-s. Zha, A. F. Goncharov, O. Tschauner, H.-k. Mao, and R. J. Hemley, In situ high-pressure x-ray diffraction study of H_2 O ice VII, J. Chem. Phys. **128**, 064510 (2008).

[12] H. Kadobayashi, H. Hirai, T. Matsuoka, Y. Ohishi, and Y. Yamamoto, A possible existence of phase change of deuterated

ice VII at about 11 GPa by X-ray and Raman studies, J. Phys.: Conf. Ser. **500**, 182017 2014).

[13] T. Meier, S. Petitgirard, S. Khandarkhaeva, and L. Dubrovinsky, Observation of nuclear quantum effects and hydrogen bond symmetrisation in high pressure ice, Nat. Commun. **9**, 1 (2018).

[14] M. Guthrie, R. Boehler, C. A. Tulk, J. J. Molaison, A. M. dos Santos, K. Li, and R. J. Hemley, Neutron diffraction observations of interstitial protons in dense ice, Proc. Natl. Acad. Sci. **110**, 10552 (2013).

[15] Z. M. Grande, C H. Pham, D. Smith, J. H. Boisvert, C. Huang, J. S. Smith, N. Goldman, J. L. Belof, O. Tschauner, J. H. Steffen, and A. Salamat, Pressure-driven symmetry transitions in dense H_2 O ice, Phys. Rev. B **105**, 104109 (2022).

[16] W. Wagner and A. Pruß, The IAPWS formulation 1995 for the thermodynamic properties of ordinary water substance for general and scientific use, J. Phys. Chem. Ref. Data **31**, 387 (2002).

[17] S. Herrig, M. Thol, A. H. Harvey, and E. W. Lemmon, A reference equation of state for heavy water, J. Phys. Chem. Ref. Data **47**, 043102 (2018).

[18] J. C. Duplan, L Mahi, and J. L. Brunet, NMR determination of the equilibrium constant for the liquid $H_2O - D_2$ O mixture, Chem. Phys. Lett. **413**, 400 (2005).

[19] Q. Hu, H. Zhao, and S. Ouyang, Understanding water structure from Raman spectra of isotopic substitution H_2O/D_2 O up to 573 K, Phys. Chem. Chem. Phys. **19**, 21540 (2017).

[20] Q. Hu, H. Zhao, and S. Ouyang, Interpreting the Raman OH/OD stretch band of ice from isotopic substitution and phase transition effects, Phys. Chem. Chem. Phys. **20**, 28600 (2018).

[21] M. Frost and S. H. Glenzer, Isotope effects on the high pressure viscosity of liquid water measured by differential dynamic microscopy, Appl. Phys. Lett. **116**, 233701 (2020).

[22] C. G. Salzmann, Advances in the experimental exploration of water's phase diagram, J. Chem. Phys. **150**, 060901 (2019).

[23] C. W. F. T. Pistorius, E. Rapoport, and J. B. Clark, Phase diagrams of H_2O and D_2O at high pressures, J. Chem. Phys. **48**, 5509 (1968).

[24] K. R. Hirsch and W. B. Holzapfel, Effect of high pressure on the raman spectra of ice VIII and evidence for ice X, J. Chem. Phys. **84**, 2771 (1986).

[25] J.-A. Queyroux, J.-A. Hernandez, G. Weck, S. Ninet, T. Plisson, S. Klotz, G. Garbarino, N. Guignot, M. Mezouar, M. Hanfland *et al.*, Melting curve and isostructural solid transition in superionic ice, Phys. Rev. Lett. **125**, 195501 (2020).

[26] L. E. Bove, R. Gaal, Z. Raza, A.-A. Ludl, S. Klotz, A. M. Saitta, A. F. Goncharov, and P. Gillet, Effect of salt on the H-bond symmetrization in ice, Proc. Natl. Acad. Sci. **112**, 8216 (2015).

[27] A. Dewaele, M. Torrent, P. Loubeyre, and M. Mezouar, Compression curves of transition metals in the Mbar range: Experiments and projector augmented-wave calculations, Phys. Rev. B **78**, 104102 (2008).

[28] See Supplemental Material at http://link.aps.org/supplemental/10.1103/PhysRevResearch.5.043166 for further details of background subtraction procedure, calculated Raman modes, and experimental full widths at half maxima for the O-H and O-D stretching features.

[29] S. J. Clark, M. D. Segall, C. J. Pickard, P. J. Hasnip, M. I. J. Probert, K. Refson, and M. C. Payne, First Principles Methods using CASTEP, Z. Kristall. **220**, 567 (2005).

[30] J. P. Perdew, K. Burke, and M. Ernzerhof, Generalized Gradient Approximation Made Simple, Phys. Rev. Lett. **77**, 3865 (1996).

[31] K. Refson, P. R. Tulip, and S. J. Clark, Variational density-functional perturbation theory for dielectrics and lattice dynamics, Phys. Rev. B **73**, 155114 (2006).

[32] P. Pruzan, J. C. Chervin, and M. Gauthier, Raman spectroscopy investigation of ice VII and deuterated ice VII to 40 GPa. disorder in ice VII, Europhys. Lett. **13**, 81 (1990).

[33] Y. Yoshimura, S. T. Stewart, M. Somayazulu, H.-k. Mao, and R. J. Hemley, High-pressure x-ray diffraction and Raman spectroscopy of ice VIII, J. Chem. Phys. **124**, 024502 (2006).

[34] M. Bernasconi, P. L. Silvestrelli, and M. Parrinello, Ab initio infrared absorption study of the hydrogen-bond symmetrization in ice, Phys. Rev. Lett. **81**, 1235 (1998).

[35] A. F. Goncharov, V. V. Struzhkin, M. S. Somayazulu, R. J. Hemley, and H.-K. Mao, Compression of ice to 210 gigapascals: Infrared evidence for a symmetric hydrogen-bonded phase, Science **273**, 218 (1996).

[36] R. G. Schireman, J. Maul, A. Erba, and M. T. Ruggiero, Anharmonic coupling of stretching vibrations in ice: a periodic VSCF and VCI description, J. Chem. Theory Comput. **18**, 4428 (2022).

[37] S. Azadi and G. J. Ackland, The role of van der waals and exchange interactions in high-pressure solid hydrogen, Phys. Chem. Chem. Phys. **19**, 21829 (2017).

[38] F. Evers and A. D. Mirlin, Anderson transitions, Rev. Mod. Phys. **80**, 1355 (2008).

[39] M. F. Sykes, D. S. Gaunt, and M. Glen, Percolation processes in three dimensions, J. Phys. A: Math. Gen. **9**, 1705 (1976).